Lifshitz transition in titanium carbide driven by a graphene overlayer

M. Krivenkov [1,*] D. Marchenko [1,*] E. Golias,[2] M. Sajedi [1] A. S. Frolov [1] J. Sánchez-Barriga [1,3] A. Fedorov [1,4,5] L. V. Yashina [1] O. Rader,[1] and A. Varykhalov [1,†]

[1]*Helmholtz-Zentrum Berlin für Materialien und Energie, BESSY II, Albert-Einstein-Strasse 15, 12489 Berlin, Germany*
[2]*MAX IV Laboratory, Lund University, 22100 Lund, Sweden*
[3]*IMDEA Nanoscience, C/ Faraday 9, Campus de Cantoblanco, 28049 Madrid, Spain*
[4]*Leibniz-Institut für Festkörper- und Werkstofforschung Dresden, Helmholtzstrasse 20, 01069 Dresden, Germany*
[5]*Joint Lab Functional Quantum Materials at BESSY II, Albert-Einstein-Strasse 15, 12489 Berlin, Germany*

Two-dimensional (2D) Dirac materials are electronically and structurally very sensitive to proximity effects. We demonstrate, however, the opposite effect: that the deposition of a monolayer 2D material could exercise a substantial influence on the substrate electronic structure. Here we investigate TiC(111) and show that a graphene overlayer produces a proximity effect, changing the Fermi surface topology of the TiC from six electron pockets to one hole pocket on the depth of several atomic layers inside the substrate. In addition, the graphene electronic structure undergoes an extreme modification as well. While the Dirac cone remains gapless, it experiences an energy shift of 1.0 eV beyond what was recently achieved for the Lifshitz transition of overdoped graphene. Due to this shift, the antibonding π^* band at the $\overline{\mathrm{M}}$ point becomes occupied and observable by photoemission.

I. INTRODUCTION

Two-dimensional (2D) materials offer the possibility to tune and dramatically change electronic properties through proximity effects. Their origin can be rather complex. Superconductivity, e.g., can be achieved not only by established proximity [1], but also by electrostatic gating [2]. The spin-orbit interaction can effectively be imposed by interlayer hybridization [3] and a nontrivial band topology can, in turn, be induced by spin-orbit proximity [4].

Due to its peculiar density of states as a Dirac material, graphene can easily be doped around its charge neutral point. Originally believed to be unattainable [5], the Lifshitz transition of monolayer graphene at the $\overline{\mathrm{M}}$-point Van Hove singularity was even achieved recently by overdoping when pushing the Dirac point 1.6 eV below the Fermi energy [6,7]. Lifshitz transitions at the $\overline{\mathrm{K}}$ point occur on a much smaller energy scale. These appear in graphene bilayers due to trigonal warping [8–10]. These transitions become extremely interesting when a superlattice effect, interlayer hybridization, and gating-induced doping are combined in twisted bilayer graphene leading to a correlated insulator phase [11], superconductivity [12], and orbital ferromagnetism [13,14]. This becomes possible because, around magic angles [15],

hybridization leads to avoided crossings creating Van Hove singularities [5], which give rise to a series of Lifshitz transitions due to the movement and annihilation of Dirac points [16]. The superconductivity was explained by nesting near the Lifshitz transition [17,18] and by the created flat bands [16].

In the present work we report another case of a proximity effect in which graphene exerts a combination of a superlattice effect, interlayer hybridization, and doping. The proximity effect is not short ranged but affects a resonance band which spreads deep below the surface. An anisotropic band-gap opening at the Fermi level transforms the *petal-shaped* Fermi surface of TiC to a *gear-shaped* contour for graphene/TiC.

TiC is an intriguing refractory ceramic with extreme mechanical hardness and melting point of 3430 K. The (111) face of TiC is known to be highly reactive and applied in catalysis [19], supercapacitors [20], and Li-air batteries [21]. Epitaxial graphene on TiC(111) [22,23] occurs in synthetic composite materials as well as in natural presolar stardust in meteorites [24,25]. Here, we prepare graphene on TiC by chemical vapor deposition as reported previously [22]. We conduct studies using low-energy electron diffraction (LEED), scanning tunneling microscopy (STM), and angle-resolved photoemission (ARPES) techniques and density functional theory (DFT) calculations.

II. STRUCTURE OF GRAPHENE ON TiC(111)

Graphene grows on TiC(111) with a lattice mismatch. This results in a moiré pattern [23,26,27] which can be easily seen in the real-space STM image in Fig. 1(b). It shows also a line profile and a Fourier transformation analysis. In the LEED pattern [Fig. 1(a)] all primary spots are surrounded
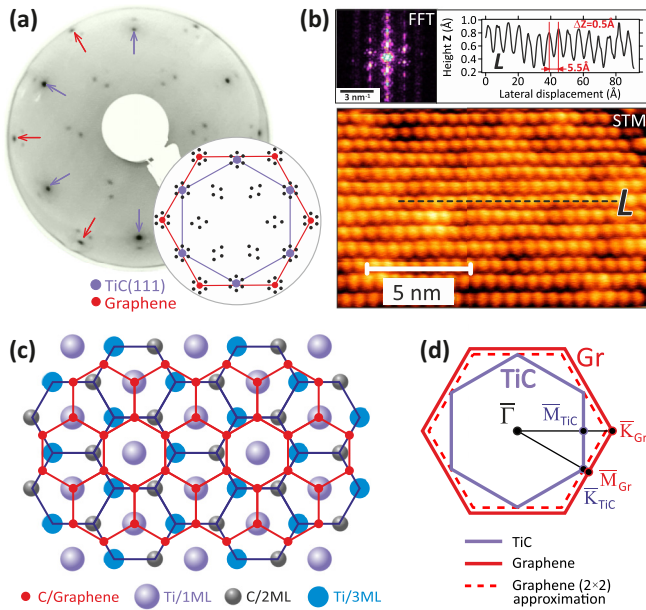

FIG. 1. Structure of graphene on TiC(111). (a) LEED pattern measured at 60 eV. Magenta arrows mark primary spots of TiC, red arrows those from graphene. (b) STM of graphene on TiC(111) with topographic profile and Fourier transformation analysis. (c) Model 2×2 atomic structure closely approximating the LEED and STM data and used in DFT calculations. (d) Surface Brillouin zones of TiC(111), graphene, and stretched graphene of the 2×2 approximation.

by hexagonal constellations of weaker spots arising from the moiré pattern. Additional stand-alone groups of spots located closer to the image center are due to double diffraction in the graphene epilayer [23,37]. From the LEED data we determine that graphene and TiC lattices have a higher-order coincidence relation: 15 graphene periods match exactly $7\sqrt{3}$ periods of the TiC lattice rotated by $30°$ [23]. This lattice, explained in detail in the Supplemental Material Fig. S1 [28], can for the present purpose be approximated by 2×2 graphene matching $(\sqrt{3} \times \sqrt{3})$ $R30°$ TiC, Fig. 1(c), in which graphene is adsorbed at the Ti-terminated [29] face of TiC with one graphene hexagon centered over Ti [30]. The use of this 2×2 graphene superstructure is, in particular, justified by the fact that, in our ARPES measurement, no features of the moiré structure are observed, but the 2×2 structure is dominant. Similar quasi-(2×2) replicas were observed in graphene on a SiC carbon buffer layer [31,32].

III. LARGE NONRIGID ENERGY SHIFT

In the band-structure measurement of graphene/TiC(111) by ARPES in Figs. 2(a) and 2(b), a substantial modification occurs as compared to ideal graphene: the bonding π band (which also forms the lower half of the Dirac cone) undergoes a nonrigid shift ΔE toward higher binding energy. ΔE at $\overline{\Gamma}_{Gr}$ amounts to ~2.25 eV, at $\overline{K}_{Gr} \sim 2.55$ eV, and at $\overline{M}_{Gr}$ even ~3.05 eV. These shifts are due to interaction with the TiC. At $\overline{M}_{Gr}$ the shift is so substantial that the antibonding π^* band becomes occupied and observable by photoemission in
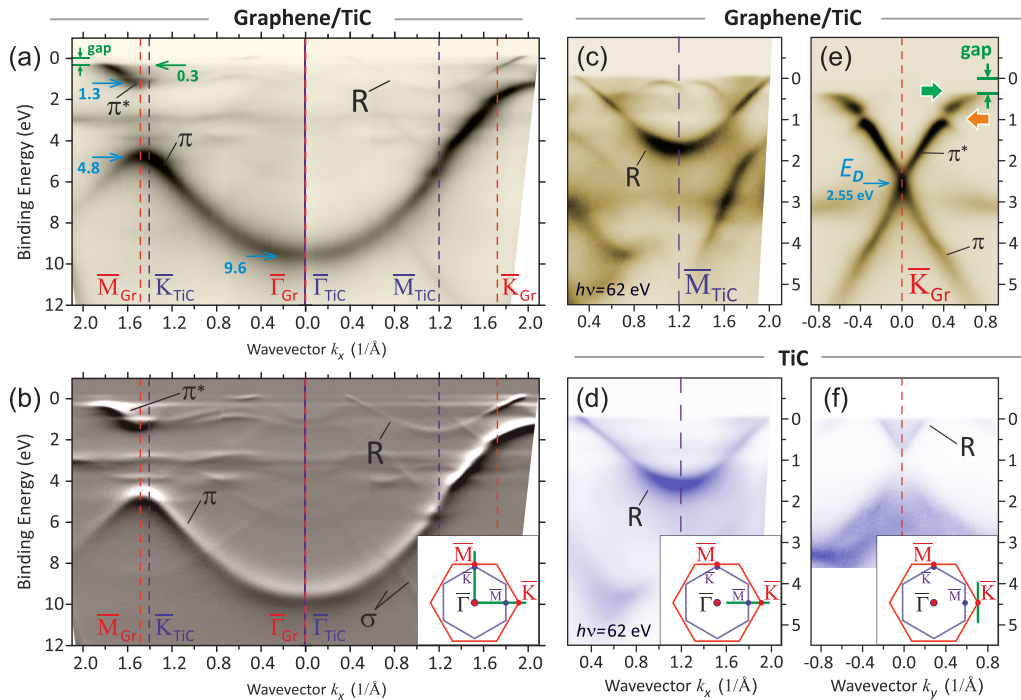
FIG. 2. Band structure of (a), (b) graphene on TiC(111) by ARPES and (c)–(f) identification of TiC bands. Measurements of (c) graphene/TiC and (d) bare TiC with purely s-polarized light (π band of graphene is suppressed due to photoemission matrix elements). (e) Dirac cone at $\overline{K}$ measured with predominantly p-polarized light. (f) The same measurement for bare TiC for comparison. Displayed are (a), (c)–(f) raw data (darker colors correspond to higher photoemission intensity) and (b) derivative $\frac{dI}{dE}$. Green and orange arrows mark hybridization gaps. Measurements are done at $h\nu = 62$ eV. Insets: Measurement directions (green lines) in the Brillouin zone of graphene (red) and TiC (blue).

the vicinity of the Fermi level which has, to our knowledge, never been observed before. This part of the band structure corresponds to the Van Hove singularity of graphene that was moved previously to the Fermi energy by heavy doping [6,7]. In the present case the shift is by 1.3 eV larger than in Ref. [6], i.e., it is moved 1.3 eV below E_F.

IV. ELECTRONIC HYBRIDIZATION

The second indication of strong interaction between graphene and TiC is that their bands hybridize. Surprisingly, the π^* band in Figs. 2(a) and 2(b) does not cross the Fermi energy, but forms a gap extending from E_F to $\sim$0.3 eV binding energy. This gap has no counterpart in the π band, meaning broken electron-hole symmetry due to the interaction with the TiC substrate. In Fig. 2(e) this hybridization gap at 0.3 eV as well as another one at 0.8 eV are marked (green and orange arrows). Taking these observations together, we identify the hybridization as responsible for the large magnitude of the energy shift ΔE (i.e., 2.2–3.0 eV) of the graphene π band. Such a giant energy shift cannot be ascribed to charge doping alone as we know from C1s core-level spectroscopy of graphene/TiC [22]. Since TiC(111) is Ti-terminated [29], the C1s develops only a small surface shift of +0.29 eV. Upon graphene deposition, this surface shift increases only slightly to +0.39 eV, which means a shift by only 0.5 eV relative to freestanding graphene [22]. Instead, we believe that more important for the shift than charge doping is the depopulation of hybrid antibonding bands due to the location of the Ti 3d states close to the Fermi level. Similarly to the case of graphene/Ni(111) [33], we expect that such depopulation causes strong covalent coupling between graphene and TiC (which is observed in C K-edge absorption [22]) which can explain the very large shift ΔE.

V. GAPLESS DIRAC POINT

We see in Fig. 2(e) that the Dirac cone of the graphene is gapless. This is surprising in view of the strong interaction with the TiC substrate evidenced by the large energy shift. That is, however, not the first such case. In graphene/Ni(111), despite strong interaction, energy shift, and sublattice symmetry breaking, no gap appears at the Dirac point [34]. Our DFT calculations also confirm the absence of the gap at the Dirac point and its replicas for graphene on TiC(111) as seen in Fig. 5(g) below 2 eV binding energy.

VI. FERMI SURFACE OF TiC AND GRAPHENE/TiC

In Fig. 2 a prominent feature is present which we labeled R. The reference measurements of bare TiC(111) in Figs. 2(d) and 2(f) show no trace of a graphene Dirac cone but the band R is present, meaning this band belongs to TiC. Photon-energy-dependent measurements are presented in the Supplemental Material Fig. S2 [28]. Figure 3 uses full photoemission mapping $I(E, k_x, k_y)$ to derive constant energy surfaces (CES) at different binding energies up to the Fermi level for bare TiC(111) (left column) and graphene/TiC (right column). Due to the strong shift ΔE we have to look at higher binding energies such as 1.7 eV to see the characteristic
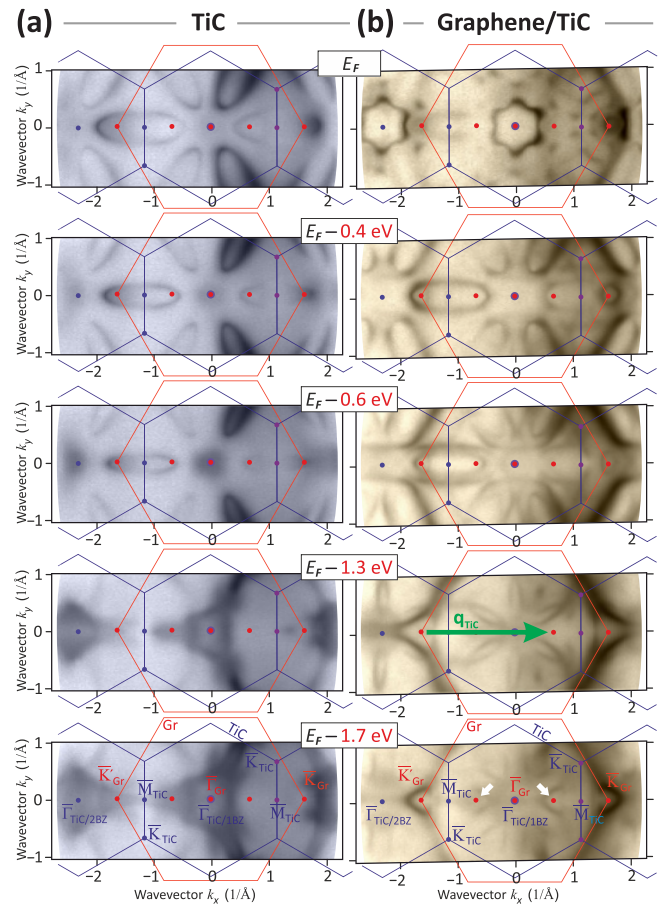

FIG. 3. Graphene-induced Lifshitz-like transition of TiC(111) revealed by comparative full photoemission mapping of the band structures of (a) bare TiC(111) and (b) graphene/TiC(111). White arrows mark two (out of totally six) graphene $\overline{K}$ point replicas with corresponding replica Dirac cones. The topmost panels show the transformation of the *petal-shaped* Fermi surface of TiC to a novel *gear-shaped* Fermi surface contour of graphene/TiC. Darker colors correspond to higher photoemission intensity. Measurements are done at $h\nu = 62$ eV.

features of graphene, the triangular contours of the π band, surrounding $\overline{K}_{Gr}$. The characteristics of TiC(111) are elliptical contours arranged in a *petal-shaped* structure close to the Fermi energy. These electron pockets are formed by the band R crossing the Fermi level.

VII. R-BAND LOCALIZATION

We investigated the R-band localization by DFT calculations (Fig. 4). The localization shows that it is neither a surface nor a bulk band, but a surface resonance with the wave function penetrating deep into the bulk of the TiC crystal. These results mean that the one-atom-thick graphene overlayer can modify not only the substrate surface but much deeper spreading states. Figure 4 shows that the charge density of the Fermi surface peaks at the third TiC layer and decays to half of its maximum at the sixth TiC layer. While this cannot change the bulk properties of TiC, the effect does have the potential to affect heterostructures even with bulk-like structural units.
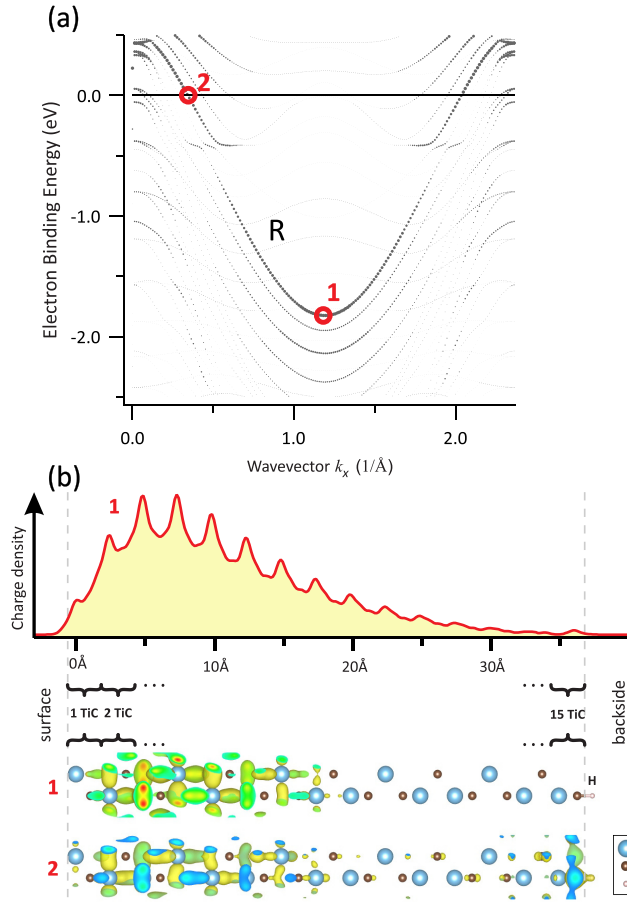
FIG. 4. DFT calculation of 15-layered TiC structure. (a) $\overline{\Gamma K}$ dispersion of the R-band, which forms the *petal-shaped* structure. Point size represents contribution of all orbitals of the second TiC layer [compare with experimental picture of Fig. 2(d)]. (b) The R-band real-space localization presented for the points marked by circles 1 and 2 in panel (a).

VIII. SIX EXTRA DIRAC CONES

The CESs in Fig. 3(b) and Supplemental Material Fig. S3(a) [28] deliver the remarkably clear picture of the Dirac band replication due to the 2×2 superstructure. In particular, it is seen (e.g., at $E_F - 1.7$ eV) that new Dirac cones appear due to a reciprocal lattice vector $\mathbf{q}_{TiC}$ of the TiC(111) (green arrow). These six new $\overline{K}$ points (three $\overline{K}_{Gr}$ and three $\overline{K}'_{Gr}$) within each SBZ of the TiC and their Dirac cones create around $\overline{\Gamma}$ another flower-shaped CES [see, e.g., $E_F - 1.7$ eV and $E_F - 1.3$ in Fig. 3(b)]. [Supplemental Material Fig. S3(b) [28] displays band-structure cuts and proves that both the primary and replica Dirac cones are intact and gapless.]

IX. LIFSHITZ-LIKE TRANSITION

The Fermi surfaces in Fig. 3 show that the *petal-shaped* electron pockets [Fig. 3(a) at E_F] undergo a transition where only the parts near the center of the Brillouin zone remain. These connect to form a *gear-shaped* hole pocket in the SBZ center [Fig. 3(b) at E_F]. With the help of the replicas we can understand this behavior in detail. We start out from energies further below the Fermi level. At $E_F - 1.7$ eV we see triangles

of the replicated graphene Dirac cones around the $\overline{K}_{Gr}$ point (white arrows). For energies towards E_F, the triangles grow and show the warping typical of graphene. At $E_F - 1.7$ eV also the ellipses of TiC start to emerge in a point, visible at $E_F - 0.6$ eV and higher as ellipses. At $E_F - 0.6$ eV one can see that the warped triangles of the graphene have a curvature that is similar to the elliptical pockets of the TiC. At $E_F - 0.4$ eV the two have almost met but at E_F most of this shape has disappeared to give rise to a Fermi surface with an altogether new topology.

X. DISCUSSION

The band dispersions along a cut through neighboring replicated $\overline{K}$ points ($\overline{K}_{Gr}$ and $\overline{K}'_{Gr}$) are presented in Fig. 5(d) for bare TiC and Fig. 5(e) for graphene/TiC. The geometry of these cuts is explained in Figs. 5(b) and 5(c), respectively [traces *L*]. The cuts were extracted from full ARPES photoemission maps. The dotted lines follow the band dispersion and show that the band of bare TiC crosses Fermi level at $\mathbf{k}_x \sim 0.1 \text{Å}^{-1}$. When, however, graphene is present on top of TiC, the TiC band gets gapped around the Fermi level (the region is marked with the green dashed circle). This causes the Fermi surface topology change.

Detailed analysis of the band dispersion modification in Figs. 5(d) and 5(e) indicates that the gap at the Fermi level and the resulting Lifshitz-like transition are formed not due to a rigid downward energy shift of the entire band. Instead, a hybridization of the TiC electronic structure with the replica of the π^* band of graphene occurs and strongly changes the band dispersion. In Fig. 5(a) we show a sketch of such transition produced by a model of crossing parabolas with zero (left), moderate (center), and strong (right) interaction parameter τ. The model is based on the Hamiltonian with $E(k_x, k_y)$ (parabolic energy dispersions) as diagonal elements, and interaction parameter τ on off-diagonal positions. Despite the simplicity of this model, it graphically explains the mechanism of the transformation from a *petal-* to a *gear-shaped* Fermi surface observed experimentally.

Figures 5(f) and 5(g) show the calculated band dispersion corresponding to the cuts *L* of Figs. 5(b) and 5(c). One can see how the presence of the graphene pulls the top part of the TiC band downwards in energy below the Fermi level without a rigid energy shift, just as observed in the experiment. To clarify this picture, a layer- and orbital-dependent analysis was performed with the results presented in Fig. 5(g). One can see a direct hybridization between graphene and substrate bands in the region of interest (green dashed circle) which fully confirms the hybridization picture that the experiment suggests.

We want to emphasize two aspects of the present experiments. We showed that the hybridization does not only cause the Fermi surface transformation but also the strong energy shift of the graphene band structure. Graphite intercalation with the double donor Ca in CaC$_6$ has consistently shown the highest T_C with 11.6 K [35] and the highest binding energy of the Dirac point of 1.5 eV [36]. Graphene monolayer overdoping has also been achieved recently [6,7]. The present Dirac point is even by 1 eV deeper in energy than in the examples presented.
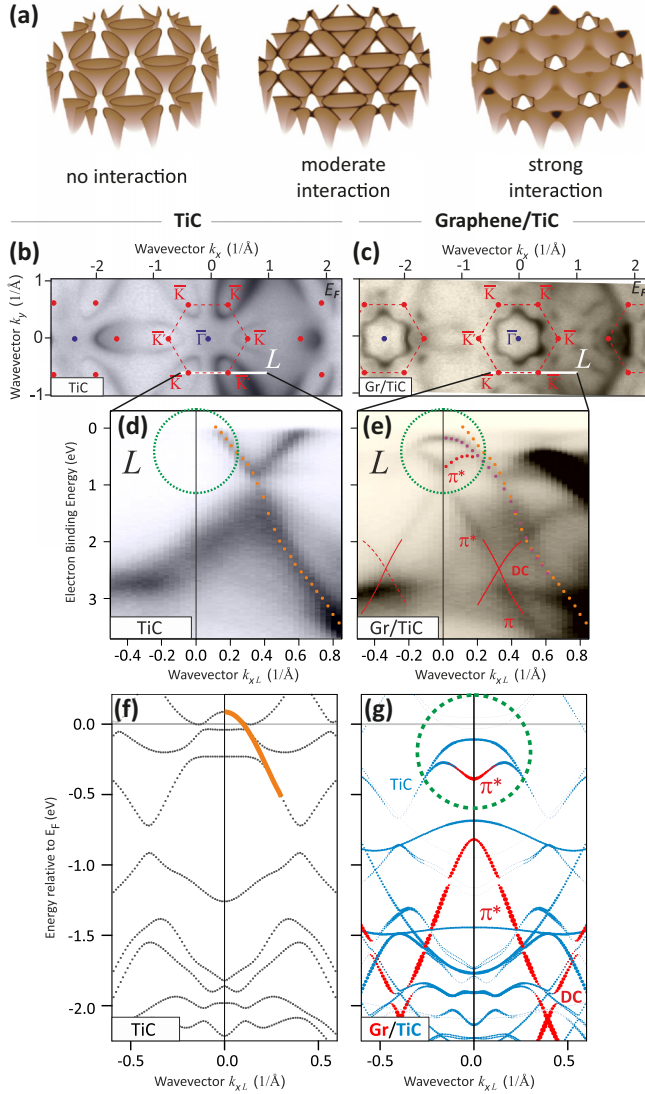
FIG. 5. (a) A graphical sketch of the Lifshitz-like transition from a *petal-shaped* Fermi surface in TiC to a *gear-shaped* hole Fermi surface. (b), (c) Corresponding experimental Fermi surfaces (log. intensity scale, black means higher intensity). White lines L indicate band-structure cuts from full photoemission maps presented in panels (d), (e) (linear intensity scale, black means higher intensity). Green circles highlight the region of interest where the Van Hove singularity appears, dotted lines follow dispersions of the bands, Dirac cone replica is marked as DC. (f), (g) DFT calculated band structures along the direction L. The TiC Fermi level position was corrected by 165 meV, graphene/TiC Fermi level is as calculated. In panel (g) contributions of graphene p_z and all orbitals of the second TiC layer are shown by the size of red and blue markers, respectively. Skipping contributions of the first layer allows to visually distinguish them.

XI. SUMMARY

We showed in detail that the graphene overlayer can lead to a proximity-induced Fermi surface transformation in TiC,

affecting a surface resonance band which spreads deep into the bulk. The effect is important for consideration beyond graphene, especially when building 2D heterostructures. For example, a hybridization on one side of a heterostructure with a state reaching through passivating or insulating layers could produce an essential electronic structure modification deep inside the conduction layer.

XII. METHODS

A. Experiment

The TiC(111) crystal was cleaned by repeated cycles of annealing in oxygen ($T = 900$ K, $p_{O_2} = 5 \times 10^{-8}$ mbar) followed by short heating up to $T = 2300$ K. Graphene was prepared by chemical vapor deposition of propylene on the TiC sample held at $T = 1200$ K according to recipes from earlier works [23,37]. Our study mainly focused on graphene/TiC(111), but we also performed comparative measurements of bare TiC(111). Although the TiC(111) surface was found to be very reactive for prolonged measurements even in an ultrahigh vacuum [38,39], we could keep it clean by frequent annealing above $T = 2000$ K and acquire very accurate ARPES data of TiC surface bands. ARPES experiments were performed at the beamline UE112-PGM2a using the end-station ARPES 1^2 equipped with a hemispherical electron analyzer (Scienta R8000) [40]. Scanning tunneling microscopy (STM) was done at room temperature with an Omicron VT STM instrument using polycrystalline tungsten tips prepared as described elsewhere [41].

B. Theory

We performed DFT calculations with the graphene lattice constant expanded by 7% to match the 2×2 structure. It is based on our own STM, LEED, and ARPES measurements and is similar to structures used in previous studies [23,30]. The Brillouin zone effect due to the lattice constant expansion is shown in Fig. 1(d). The unit cell used in calculations and the corresponding Brillouin zones of graphene, titanium carbide and their superlattice is presented in Supplementary Material Fig. S4 [28]. The VASP package [42] was used for structural optimization and band structure calculations. We employed the projector augmented wave method [43] and the semilocal Perdew-Burke-Ernzerhof approximation to the exchange-correlation energy [44]. The electronic orbitals were expanded using a plane-wave basis with kinetic energies up to 450 eV, a 11×11 Monkhorst-Pack grid [45] was used for the sampling of the basal reciprocal plane, and nonlocal dispersive van der Waals interactions were taken into account with the DFT-D2 method of Grimme [46].

All data needed to evaluate the conclusions in the paper are present in the paper and/or the Supplementary Materials [28]. Additional data related to this paper may be requested from the authors.

[1] P. G. De Gennes, Boundary effects in superconductors, Rev. Mod. Phys. **36**, 225 (1964).

[2] D. Costanzo, S. Jo, H. Berger, and A. F. Morpurgo, Gate-induced superconductivity in atomically thin MoS_2 crystals, Nat. Nanotechnol. **11**, 339 (2016).

[3] D. Marchenko, A. Varykhalov, M. R. Scholz, G. Bihlmayer, E. I. Rashba, A. Rybkin, A. M. Shikin, and O. Rader, Giant Rashba splitting in graphene due to hybridization with gold, Nat. Commun. **3**, 1232 (2012).

[4] T. Frank, P. Högl, M. Gmitra, D. Kochan, and J. Fabian, Protected Pseudohelical Edge States in Z_2-Trivial Proximitized Graphene, Phys. Rev. Lett. **120**, 156402 (2018).

[5] G. Li, A. Luican, J. M. B. Lopes dos Santos, A. H. Castro Neto, A. Reina, J. Kong, and E. Y. Andrei, Observation of Van Hove singularities in twisted graphene layers, Nat. Phys. **6**, 109 (2010).

[6] J. L. McChesney, A. Bostwick, T. Ohta, Th. Seyller, K. Horn, J. González, and E. Rotenberg, Extended van Hove Singularity and Superconducting Instability in Doped Graphene, Phys. Rev. Lett. **104**, 136803 (2010).

[7] P. Rosenzweig, H. Karakachian, D. Marchenko, K. Küster, and U. Starke, Overdoping Graphene Beyond the van Hove Singularity, Phys. Rev. Lett. **125**, 176403 (2020).

[8] E. McCann and V. I. Falko, Landau-Level Degeneracy and Quantum Hall Effect in a Graphite Bilayer, Phys. Rev. Lett. **96**, 086805 (2006).

[9] Y. Lemonik, I. L. Aleiner, C. Toke, and V. I. Falko, Spontaneous symmetry breaking and Lifshitz transition in bilayer graphene, Phys. Rev. B **82**, 201408(R) (2010).

[10] A. Varlet, D. Bischoff, P. Simonet, K. Watanabe, T. Taniguchi, T. Ihn, K. Ensslin, M. Mucha-Kruczyński, and V. I. Fal'ko, Anomalous Sequence of Quantum Hall Liquids Revealing a Tunable Lifshitz Transition in Bilayer Graphene, Phys. Rev. Lett. **113**, 116602 (2014).

[11] Y. Cao, V. Fatemi, A. Demir, S. Fang, S. L. Tomarken, J. Y. Luo, J. D. Sanchez-Yamagishi, K. Watanabe, T. Taniguchi, E. Kaxiras, R. C. Ashoori, and P. Jarillo-Herrero, Correlated insulator behaviour at half-filling in magic-angle graphene superlattices, Nature (London) **556**, 80 (2018).

[12] Y. Cao, V. Fatemi, S. Fang, K. Watanabe, T. Taniguchi, E. Kaxiras, and P. Jarillo-Herrero, Unconventional superconductivity in magic-angle graphene superlattices, Nature (London) **556**, 43 (2018).

[13] A. L. Sharpe, E. J. Fox, A. W. Barnard, J. Finney, K. Watanabe, T. Taniguchi, M. A. Kastner, and D. Goldhaber-Gordon, Emergent ferromagnetism near three-quarters filling in twisted bilayer graphene, Science **365**, 605 (2019).

[14] M. Serlin, C. L. Tschirhart, H. Polshyn, Y. Zhang, J. Zhu, K. Watanabe, T. Taniguchi, L. Balents, and A. F. Young, Intrinsic quantized anomalous Hall effect in a moiré heterostructure, Science **367**, 900 (2019).

[15] R. Bistritzer and A. H. MacDonald, Moiré bands in twisted double-layer graphene, Proc. Natl. Acad. Sci. USA **108**, 12233 (2011).

[16] C. Xu and L. Balents, Topological Superconductivity in Twisted Multilayer Graphene, Phys. Rev. Lett. **121**, 087001 (2018).

[17] C.-C. Liu, Li-Da Zhang, W.-Q. Chen, and F. Yang, Chiral Spin Density Wave and $d + id$ Superconductivity, Phys. Rev. Lett. **121**, 217001 (2018).

[18] M. Fleischmann, R. Gupta, F. Wullschläger, S. Theil, D. Weckbecker, V. Meded, S. Sharma, B. Meyer, and S. Shallcross, Perfect and controllable nesting in minimally twisted bilayer graphene, Nano Lett. **20**, 971 (2020).

[19] X. Chu, Z. Fu, S. Li, X. Zhang, and Z. Yang, Effects of a TiC substrate on the catalytic activity of Pt for NO reduction, Phys. Chem. Chem. Phys. **18**, 13304 (2016).

[20] M. Ghidiu, M. R. Lukatskaya, M.-Q. Zhao, Y. Gogotsi, and M. W. Barsoum, Conductive two-dimensional titanium carbide 'clay' with high volumetric capacitance, Nature (London) **516**, 78 (2014).

[21] A. Ya. Kozmenkova, E. Yu. Kataev, A. I. Belova, M. Amati, L. Gregoratti, J. Velasco-Vélez, A. Knop-Gericke, B. Senkovsky, D. V. Vyalikh, D. M. Itkis, Y. Shao-Horn, and L. V. Yashina, Tuning surface chemistry of TiC electrodes for lithium-air batteries, Chem. Mater. **28**, 8248 (2016).

[22] E. Yu. Kataev, D. Yu. Usachov, A. S. Frolov, A. A. Rulev, A. A. Volykhov, A. Ya. Kozmenkova, M. Krivenkov, D. Marchenko, A. Varykhalov, M. V. Kuznetsov, D. Vyalikh, and L. V. Yashina, Native and graphene-coated flat and stepped surfaces of TiC, Carbon **132**, 656 (2018).

[23] H. Itoh, T. Ichinose, C. Oshima, T. Ichinokawa, and T. Aizawa, Scanning tunneling microscopy of monolayer graphite epitaxially grown on a TiC(111) surface, Surf. Sci. Lett. **254**, L437 (1991).

[24] G. von Helden, A. G. G. M. Tielens, D. van Heijnsbergen, M. A. Duncan, S. Hony, L. B. F. M. Waters, and G. Meijer, Titanium carbide nanocrystals in circumstellar environments, Science **288**, 313 (2000).

[25] Y. Kimura and C. Kaito, Titanium carbide particles as pre-solar grains, Mon. Not. R. Astron. Soc. **343**, 385 (2003).

[26] K. Kobayashi, Y. Souzu, N. Isshiki, and M. Tsukada, Theory of STM images of monolayer graphite on transition-metal surface, Appl. Surf. Sci. **60-61**, 443 (1992).

[27] K. Kobayashi, Moiré pattern in scanning tunneling microscopy of monolayer graphite, Phys. Rev. B **50**, 4749 (1994).

[28] See Supplemental Material at http://link.aps.org/supplemental/10.1103/PhysRevResearch.5.023120 for information on Gr/TiC(111) unit cell, surface Brillouin zone, and additional ARPES data, including photon energy dependent measurements.

[29] K. E. Tan, M. W. Finnis, A. P. Horsfield, and A. P. Sutton, Why TiC(111) is observed to be Ti terminated, Surf. Sci. **348**, 49 (1996).

[30] K. Kobayashi and M. Tsukada, Electronic structure of monolayer graphite on a TiC(111) surface, Phys. Rev. B **49**, 7660 (1994).

[31] K. Nakatsuji, Y. Shibata, R. Niikura, F. Komori, K. Morita, and S. Tanaka, Shape, width, and replicas of π bands of single-layer graphene grown on Si-terminated vicinal SiC(0001), Phys. Rev. B **82**, 045428 (2010).

[32] F. Bisti, G. Profeta, H. Vita, M. Donarelli, F. Perrozzi, P. M. Sheverdyaeva, P. Moras, K. Horn, and L. Ottaviano, Electronic and geometric structure of graphene/SiC(0001) decoupled by lithium intercalation, Phys. Rev. B **91**, 245411 (2015).

[33] A. A. Popova, A. M. Shikin, A. G. Rybkin, D. E. Marchenko, O. Yu. Vilkov, A. A. Makarova, A. Yu. Varykhalov, and O. Rader, The role of the covalent interaction in the formation of

the electronic structure of Au- and Cu-intercalated graphene on Ni(111), Phys. Solid State **53**, 2539 (2011).

[34] A. Varykhalov, D. Marchenko, J. Sánchez-Barriga, M. R. Scholz, B. Verberck, B. Trauzettel, T. O. Wehling, C. Carbone, and O. Rader, Intact Dirac Cones at Broken Sublattice Symmetry: Photoemission Study of Graphene on Ni and Co, Phys. Rev. X **2**, 041017 (2012).

[35] T. E. Weller, M. Ellerby, S. S. Saxena, R. P. Smith, and N. T. Skipper, Superconductivity in the intercalated graphite compounds C_6Yb and C_6Ca, Nat. Phys. **1**, 39 (2005).

[36] T. Valla, J. Camacho, Z.-H. Pan, A. V. Fedorov, A. C. Walters, C. A. Howard, and M. Ellerby, Anisotropic Electron-Phonon Coupling and Dynamical Nesting on the Graphene Sheets in Superconducting CaC_6 using Angle-Resolved Photoemission Spectroscopy, Phys. Rev. Lett. **102**, 107007 (2009).

[37] A. Nagashima, K. Nuka, H. Itoh, T. Ichinokawa, and C. Oshima, Electronic states of monolayer graphite formed on TiC(111) surface, Surf. Sci. **291**, 93 (1993).

[38] S. Zaima, Y. Shibata, H. Adachi, C. Oshima, S. Otani, M. Aono, and Y. Ishizawa, Atomic chemical composition and reactivity of the TiC(111) surface, Surf. Sci. **157**, 380 (1985).

[39] K. Edamoto, T. Anazawa, A. Mochida, T. Itakura, E. Miyazaki, H. Kato, and S. Otani, Angle-resolved photoemission study of the surface state on TiC(111), Phys. Rev. B **46**, 4192 (1992).

[40] A. Varykhalov, 1^2-ARPES: The ultra-high-resolution photoemission station at the U112-PGM-2a-1^2 beamline at BESSY II, J. Large-scale Res. Facilities **4**, A128 (2018).

[41] A. Varykhalov, O. Rader, and W. Gudat, Structure and quantum-size effects in a surface carbide: W(110)/C-R(15×3), Phys. Rev. B **72**, 115440 (2005).

[42] G. Kresse and J. Hafner, *Ab initio* molecular dynamics for liquid metals, Phys. Rev. B **47**, 558 (1993).

[43] P. E. Blöchl, Projector augmented-wave method, Phys. Rev. B **50**, 17953 (1994).

[44] J. P. Perdew, K. Burke, and M. Ernzerhof, Generalized Gradient Approximation Made Simple, Phys. Rev. Lett. **77**, 3865 (1996).

[45] H. J. Monkhorst and J. D. Pack, Special points for Brillouin-zone integrations, Phys. Rev. B **13**, 5188 (1976).

[46] S. Grimme, Semiempirical GGA-type density functional constructed with a long-range dispersion correction, J. Comput. Chem. **27**, 1787 (2006).